Frontal Lobe Connectivity and Network Community Characteristics are Associated with the Outcome of Subthalamic Nucleus Deep Brain Stimulation in Patients with Parkinson's Disease

Nabin Koirala[1] · Vinzenz Fleischer[1] · Martin Glaser[2] · Kirsten E. Zeuner[3] · Günther Deuschl[3] · Jens Volkmann[4] · Muthuraman Muthuraman[1] · Sergiu Groppa[1]

Abstract Deep brain stimulation (DBS) of the subthalamic nucleus (STN) is nowadays an evidence-based state of the art therapy option for motor and non-motor symptoms in patients with Parkinson's disease (PD). However, the exact anatomical regions of the cerebral network that are targeted by STN–DBS have not been precisely described and no definitive pre-intervention predictors of the clinical response exist. In this study, we test the hypothesis that the clinical effectiveness of STN–DBS depends on the connectivity profile of the targeted brain networks. Therefore, we used diffusion-weighted imaging (DWI) and probabilistic tractography to reconstruct the anatomical networks and the graph theoretical framework to quantify the connectivity profile. DWI was obtained pre-operatively from 15 PD patients who underwent DBS (mean age = 67.87 ± 7.88, 11 males, H&Y score = 3.5 ± 0.8) using a 3T MRI scanner (Philips Achieva). The pre-operative connectivity properties of a network encompassing frontal, prefrontal cortex and cingulate gyrus were directly linked to the postoperative clinical outcome. Eccentricity as a topological-characteristic of the network defining how cerebral regions are embedded in relation to distant sites correlated inversely with the applied voltage at the active electrode for optimal clinical response. We found that network topology and pre-operative connectivity patterns have direct influence on the clinical response to DBS and may serve as important and independent predictors of the postoperative clinical outcome.

Keywords Parkinson's disease · Deep brain stimulation · Structural connectivity · Community structures · Network analysis

Abbreviations

AAL	Automated anatomical labeling
AUC	Area under the curve
BCT	Brain connectivity toolbox
COG	Center of gravity
DBS	Deep brain stimulation
DWI	Diffusion-weighted imaging
FWHM	Full width at half maximum
H & Y	Hoehn and Yahr
MED OFF/ON	Medication off/on
MPRAGE	Magnetization-prepared rapid gradient-echo
ROC	Receiver operating characteristic
ROI	Region of interest
SMA	Supplementary motor area
STN	Subthalamic nucleus
UPDRS	Unified Parkinson's disease rating scale
VTA	Volume of tissue activation

Introduction

Parkinson's disease is one of the most common neurodegenerative diseases with no permanent cure. Deep brain

Muthuraman Muthuraman and Sergiu Groppa have contributed equally.

✉ Sergiu Groppa
segroppa@uni-mainz.de

[1] Department of Neurology, Johannes Gutenberg University, 55131 Mainz, Germany

[2] Department of Neurosurgery, Johannes Gutenberg University, 55131 Mainz, Germany

[3] Department of Neurology, University of Kiel, 24105 Kiel, Germany

[4] Department of Neurology, University of Würzburg, 97080 Würzburg, Germany

stimulation of the subthalamic nucleus (STN–DBS) is currently a standard evidence-based treatment for PD patients that substantially improves the motor and non-motor symptoms (Weaver et al. 2012; Odekerken et al. 2013; Klingelhoefer et al. 2014). Despite the clear clinical benefits, the STN–DBS mechanisms remain unclear (Udupa and Chen 2015). Furthermore, the STN target and the activity within it do not have an unequivocal justification for the clinical response. Earlier studies presented evidence that the stimulation might modulate the neuronal activity within the STN, while recent studies showed that the DBS rather targets the fibers entering, exiting or passing the stimulation region and not just the STN itself (McIntyre and Hahn 2010; Nambu and Chiken 2015). Moreover, the modulation of the pathological oscillations in distinct brain networks might be a critical feature of the DBS-induced clinical response (Stein and Bar-Gad 2013; Brittain and Brown 2014). Studies on primates and recent studies on humans attested the existence of the so-called hyperdirect cortical STN projections which might be of special importance for the effects of STN–DBS (Brunenberg et al. 2012a; Haynes and Haber 2013).

Apart from the therapeutic benefit, DBS can cause severe adverse effects. These effects might be long-term and complex like the cognitive decline and neuro-psychiatric symptoms which occur with STN–DBS (Fukaya and Yamamoto 2015). Hence, the understanding of the local and systemic interactions, together with an exact description of the targeted cerebral network would markedly advance our therapeutic strategies and improve the efficacy and reliability and reduce the side effects of actual DBS protocols by refining the patient selection and developing improved targeting strategies.

We hypothesize that the preoperative connectivity pattern of the interconnected regions is closely related to the clinical effectiveness of STN–DBS. Therefore, we use diffusion-weighted imaging (DWI) and probabilistic tractography to reconstruct the anatomical networks and the graph theoretical framework to quantify their connectivity profile. Network topology properties defined within graph theoretical analyses have become important measurable characteristics that explain healthy brain dynamics and help to understand and model brain disorders (Bullmore and Sporns 2009). The study of network characteristics in PD using graph theory in structural MRI has revealed specific global and local functional network topological changes characterized by a decrease in clustering and path length between the nodes in comparison to healthy controls (Olde Dubbelink et al. 2014). Additionally, structural network analysis using cortical and subcortical anatomical measurements has shown larger characteristic path length and reduced global efficiency in addition to a lower regional efficiency in frontal and parietal regions for mild cognitive impaired PD patients compared to healthy controls. This provides support for the role of aberrant network topology in motor and cognitive impairment in patients with early PD (Pereira et al. 2015). In this study, we link brain network properties with the postoperative clinical outcome to test the hypothesis that the clinical response to STN–DBS depends on the connectivity pattern of the interconnected brain regions and stimulation site.

Methods

Subjects and Data Acquisitions

In this study, fifteen patients (4 females and 11 males) with idiopathic PD without dementia and receiving DBS treatment were selected with a mean age of 67.87 ± 7.88 years. For all patients, a high resolution T1-image of the brain using MPRAGE sequence (TR = 7.7 ms, TE = 3.6 ms, flip angle = 8°, 160 slices) was obtained with a 3T MR-Scanner (Philips Achieva) using an 8-channel SENSE head coil before the DBS surgery. DWI of the whole brain at 2 mm isometric voxel resolution covering a field of view of 224×224 mm was obtained. We recorded three acquisitions of DWI sequences encompassing 32 gradient directions and five b0 (no diffusion weighting) images for each acquisition (b value = 1000s/mm^2, TE = 59 ms, TR = 11,855 ms, fat saturation "on", 60 contiguous slices). The total acquisition time for the whole protocol was 35 min which included 24 min (3×8 min) for DWI sequences. On the first postoperative day a further MRI acquisition was performed on a 1.5 T scanner (Philips Achieva, Philips Medical Systems, Best, The Netherlands) with a protocol consisting of a T1-weighted structural image of the whole brain using a standard MPRAGE sequence (TR = 10.7 ms, TE = 1.96 ms, flip angle = 8°).

Stimulation Parameters

The surgical procedure is previously explained in detail elsewhere (Groppa et al. 2014). All patients were implanted with bilateral STN electrodes (model 3389 DBS, Medtronic) and pulse generators (Activa® PC, biphase stimulation) with a pulse setting of 60 µs at 130 Hz. DBS electrode voltage is the stimulation intensity at the active electrode as expressed in Volts for the optimal clinical response. The voltage was adjusted for each individual patient while the remaining stimulation parameters (pulse width and stimulation frequency) were left unchanged. The stimulation adjustment was performed by clinicians who were blinded to the hypothesis and goals of this study, and values from the follow-up at 3 months after the implantation were included in the analysis. We choose this time point since no more impedance changes occur at this post-operative period and voltage values remain constant. The medical treatment was

individualized after DBS according to the clinical indication. The study protocol used was approved by the local ethics committee and all patients signed a written consent regarding the procedure. The clinical details are shown in Table 1.

Data Analysis and Network Reconstruction

The obtained images were preprocessed using inbuilt functionality in FSL described in detail elsewhere (Jenkinson and Smith 2001; Jenkinson et al. 2002; Johansen-Berg et al. 2004; Behrens et al. 2007). In brief, susceptibility and motion artefacts correction and diffusion tensor modelling were performed using the diffusion toolbox (topup and FDT, part of FSL). Crossing fibers distribution was estimated using BEDPOSTX (implemented in FSL) and the probability of major (f1) and secondary (f2) fiber directions were calculated. All images were aligned and affine-transformed into the stereotactic space MNI-152. A multi-fiber model was fit to the diffusion data at each voxel, allowing for tracing of fibers through regions of crossing or complexity. Here, we drew 5000 streamline samples from each seed voxel to form an estimate of the probability distribution of connections from each seed voxel. When these streamlines reach a voxel in which more than one direction is estimated, they follow the direction that is closest to the direction at which the streamline arrives. Tracts generated are volumes wherein values at each voxel represent the number of samples (or streamlines) that passed through that voxel. Here each tract from every seed mask in the atlas is repeatedly sampled and only those tracts which passed through at least one other seed mask were retained. The obtained streamlines were then used to build the connectivity matrix. For the elimination of spurious connections, tractography in individual subjects was thresholded to include only voxels through which at least 10 percent of all streamline samples had passed. A connectivity matrix was obtained using the seed masks for 116 regions of interest (ROI) defined by the Automated Anatomical Labeling atlas (Tzourio-Mazoyer et al. 2002) for each subject (Fig. 1). The links or the entries in the connectivity matrix represent the ratio of number of samples (or streamlines) that passes through ROI (j) to all generated streamlines from ROI (i). This weighted connectivity index between ROIs in the matrix was then analyzed using various network measures (both global and local) obtained via Brain Connectivity Toolbox (Rubinov and Sporns 2010) (https://sites.google.com/site/bctnet/).

Table 1 Clinical detail. Clinical parameters assessed before and after the DBS surgery

Parkinson's disease patients (n = 15)	mean ± SD
Sex (male/female)	11/4
Age (years)	67.8 ± 7.8
Disease duration (years)	13.6 ± 6.5
Preoperative Hoehn–Yahr stage (Med OFF)	3.8 ± 0.8
Preoperative Hoehn–Yahr stage (Med ON)	2.7 ± 0.5
Preoperative UPDRS $_{III}$ (Med OFF)	34.5 ± 8.4
Preoperative UPDRS $_{III}$ (Med ON)	17.4 ± 9.0
Preoperative dose of levodopa or equivalent (mg/day)	827 ± 397.0
Postoperative dose of levodopa or equivalent (mg/day)	335 ± 202.6

Here SD is the standard deviation

Community Analysis

In the reconstructed network we aimed to detect interconnected regions forming functionally relevant entities such as modules. Modules are groups of nodes that have more connections within themselves than expected in a randomly sampled group of nodes (Meunier et al. 2009). Module detection performs a partitioning of the brain into entities with higher within, than between module correlations (Girvan and Newman 2002; Newman 2006). The modules were identified using the Louvain modularity algorithm as implemented in BCT (Blondel et al. 2008) for each individual subject connectivity matrix. We performed 5000 iterations with the Louvain algorithm and the assignment of each region to a particular module was based on the maximum number of times/iterations a region was assigned to a module (Ritchey et al. 2014).

Random Network Formation and Comparison

The network measures (see below) were computed in the obtained modules. To depict neurobiologically meaningful network properties we compared the values obtained from each module with values from generated random networks. The random network was formed by weight reshuffling technique (Opsahl et al. 2008) for each individual subject. The procedure reshuffles the weights globally in the network but maintains the topology of the observed network (also for each module) and permits a distinct delineation to the development of neurodegeneration that leads to a loss of distinct topology patterns in patients.

Network Measures

In this study we assessed three network measures: characteristic path length, eccentricity and global efficiency. For a given network, these measures can characterize the efficiency of information transfer at different levels and reveal the importance of distinct regions within the module.

Characteristic path length is the average shortest distance between the regions in the network and is a measure of global integration (Stam et al. 2009). Global efficiency has been introduced as a network integration parameter to

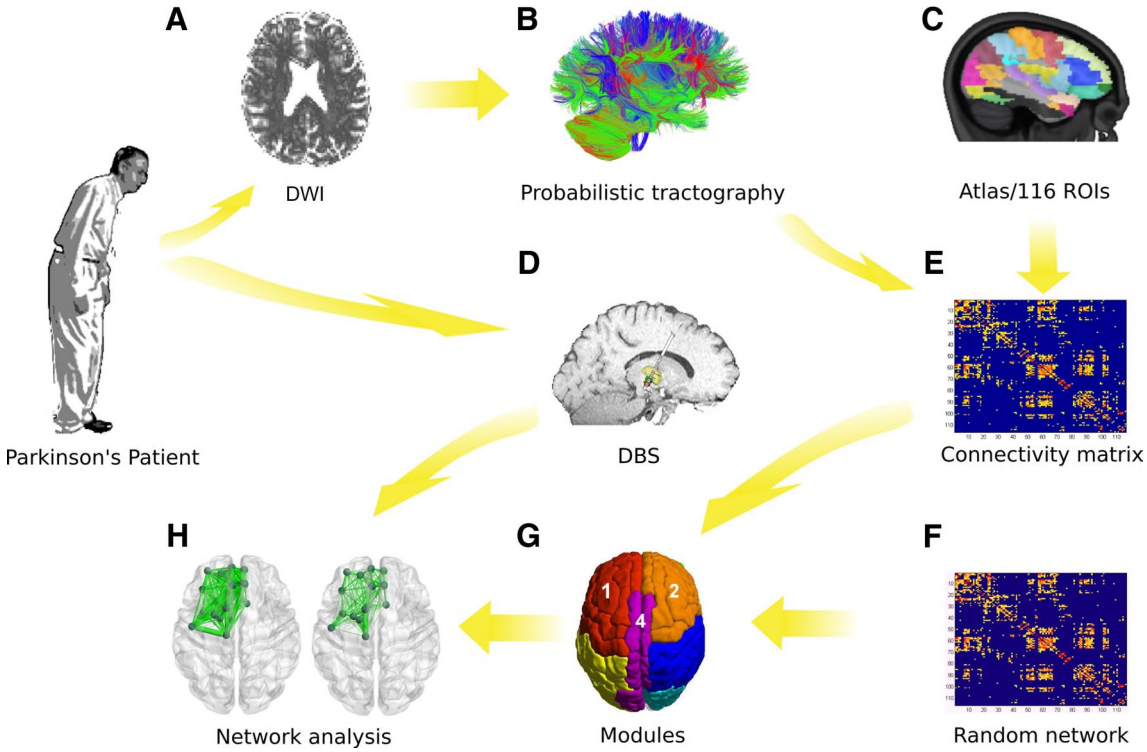

Fig. 1 Overview of methods. **a** Preoperative DWI obtained from 15 Parkinson's patients. **b** Probabilistic tractography was used to obtain the connectivity matrix using 116 ROIs as depicted in **c. d** Illustration of DBS electrodes in STN which was performed in all 15 patients. **e** The connectivity matrix with the probability from a seed region to another region. **f** The random network connectivity matrix obtained by weight reshuffling of the obtained matrix. **g** Subdivision of the whole brain into various modules using the Louvain algorithm (gamma = 2) represented by different colors. **h** Visualization of the network comparison performed between the random network and the obtained network indicating various network analyses performed

describe information flow over the entire network and is computed as the average inverse shortest path length. Even though global efficiency and characteristic path length are very similar measures, here we selected both as characteristic path length could possibly be more influenced by disconnected or remote nodes, while global efficiency is more robust to such extremes (Latora and Marchiori 2001). Eccentricity is defined as the maximal shortest path length between any two regions in the network and is a measure of relative nodal importance (Sporns 2003).

Predicting Anatomical Regions in the Networks

To establish the role of network modules and distinct anatomical regions within the module, we designed a receiver operating characteristic (ROC) curve-based analysis. Therefore, we tested how the connectivity profile of each region is ranked in comparison to others by comparing the areas under the curve (AUC). The ROC curves were obtained using the eccentricity values of the analyzed module and compared against values from the same module obtained from the random network. Moreover, for the selection of these involved modules, only those modules with an AUC above the threshold of no discrimination (i.e. greater than 0.5), and having a significantly (one sided t-test, $p < 0.05$) higher network measures value than in the generated random networks were considered. This approach ascertained the modules and regions within the module, for each network measure, with the strongest association to the outcome variable (i.e. improvement in the motor UPDRS score or DBS voltage) and having preserved network topology that differs from random networks. Furthermore in this study, we concatenated the side-specific and axial values of $UPDRS_{III}$ value to obtain a complete evaluation of the clinical outcome. Since the significant areas were not side specific and we aimed to develop universal measures that can be implemented in the clinical practice without a priori bias of handiness and laterality of the symptoms, we opted to perform whole brain analysis.

Determination of Contact-Specific Masks

Electrode positions and electrode trajectory were determined using post-operation T1 images. The detailed procedure is explained elsewhere (Witt et al. 2013). Briefly, the lead was mathematically modelled by a straight line along the

electrode trajectory. Based on the optimized lead position the T1 intensity profile was extracted along the trajectory and the electrode contact positions were then determined by observing the intensity dip apparent in the extracted intensity profile. Geometrically determined electrode contact positions were used to create spatially Gaussian weighting masks (Fig. 2). Gaussian weights were determined by specifying the following two standard deviations: (i) along the lead to model contact dimensions, known from manufacturer's annotations; (ii) from the two other orthogonal directions to model the stimulation depth. We restricted our analysis to one different mask extension: a Gaussian shape with 2 standard deviations along the lead and 2 standard deviations in depth (corresponds to an isometric mask with 4.7 mm full width at half maximum (FWHM), corresponding to a radius of ca. 2.35 mm). The multivariate Gaussians were centered at the exact contact positions. These volumes were selected considering existing literature that attest that neural elements up to a distance of 2 mm from the active contact might be reached by the studied DBS stimulation settings (Ranck 1975). The target coordinates for STN were defined relative to the midpoint of the anterior and posterior commissure [mid AC PC] on the T1 MPRAGE images used for stereotactic planning. To assess if the position of the electrodes in each patient has an effect on voltage applied or the post-operative UPDRS, we computed the geodesic distance of each calculated center of gravity (COG) of the generated electrode volume of tissue activation (VTA) masks from the obtained STN position and stereotactic target and hence correlated it with the DBS parameters (collective $UPDRS_{III}$ values and DBS voltage).

Statistical Analysis

The significant difference between the values obtained for each module in the analyzed network and the random network generated was assessed by performing a t-test ($p < 0.05$). The correlations between the obtained network measures and DBS clinical parameters were obtained using Pearson's correlation coefficient. To ascertain the significance of the correlation obtained, further leave-one-out analysis was performed. Finally, ROC curve analysis was performed to compare the connectivity profile of the modules with strongest association to the clinical outcome. All of the statistical analyses were performed using MATLAB (ver. 2013, Mathworks, Inc.).

Results

Clinical Assessment

We included 15 patients with PD who were selected for STN–DBS therapy. The $UPDRS_{III}$ scores improved after DBS–STN in both MED OFF [Before: 34.46 ± 8.35, After: 13.86 ± 5.99 ($t = 7.75$, $p < 0.001$)] and MED ON state [Before: 17.4 ± 9.03, After: 11.54 ± 5.77 ($t = 2.09$, $p < 0.05$)]. The H & Y scale scores improved after DBS–STN in MED OFF state from 3.8 ± 0.78 to 2.7 ± 0.48 ($t = 3.76$, $p < 0.01$), and in MED ON state from 2.75 ± 0.54 to 1.9 ± 0.51 ($t = 3.59$, $p < 0.01$).

Community Detection

Community detection using the Louvain algorithm depicted 10 modules encompassing the regions shown in Fig. 3. The ROC curve analysis indicated that 6 of these modules had an AUC significantly above the threshold of no-discrimination (Table 2). Significant differences in the analyzed network measures in comparison with the generated random networks were attested in two modules: *Left-frontal* and *Central*, signifying cerebral regions with preserved anatomical architecture. *Left-frontal* comprises primarily the prefrontal cortical regions of the left

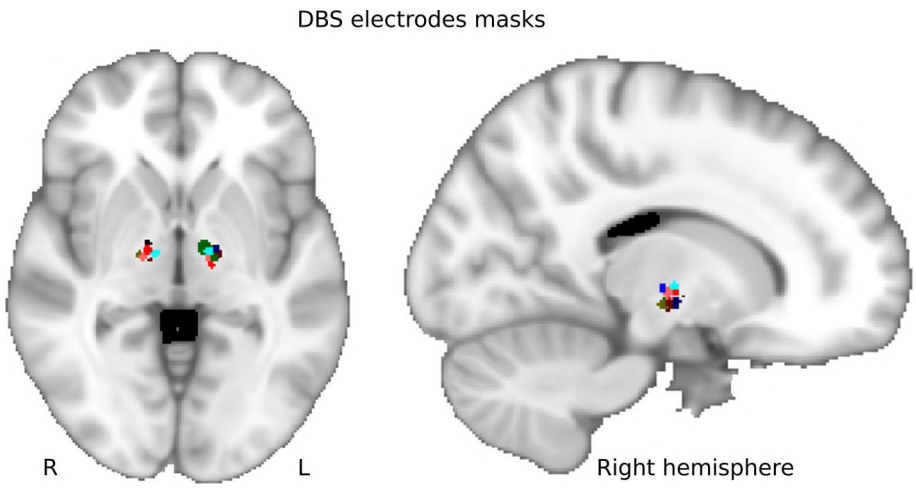

Fig. 2 DBS electrode VTA masks. The Gaussian weighted masks overlaid in MNI152-1 mm standard template for all patients. '*L*' and '*R*' represent the left and right hemisphere respectively

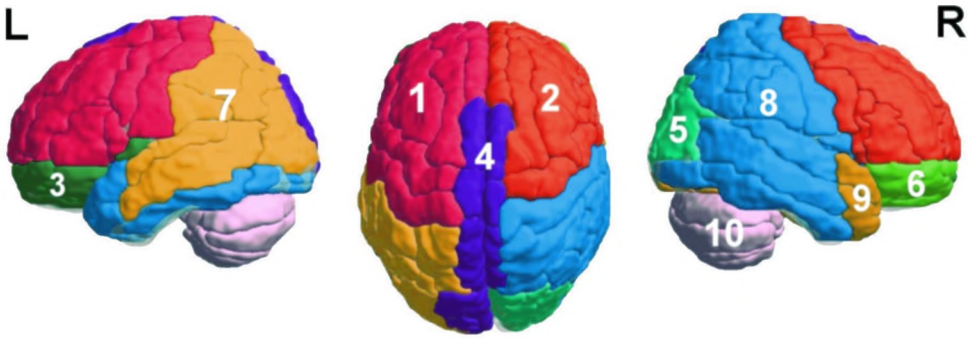

Fig. 3 Modules visualization. The whole brain subdivided into various modules using the Louvain algorithm (gamma = 2) represented by different colors. Anatomical annotations are presented in Table 2

Table 2 Modules and ROIs. Regions of Interest (ROIs) from AAL atlas assigned to the 10 modules obtained using the Louvain algorithm as visualized in Fig. 2

1. Left frontal	4. Central	Putamen_R
Precentral_L	Supp_Motor_Area_L	Pallidum_R
Frontal_Sup_L	Supp_Motor_Area_R	Thalamus_R
Frontal_Mid_L	Cingulum_Mid_L	Heschl_L
Frontal_Inf_Oper_L	Cingulum_Mid_R	Temporal_Sup_L
Frontal_Inf_Tri_L	Cingulum_Post_L	Temporal_Mid_L
Frontal_Sup_Medial_L	Cingulum_Post_R	8. Left parieto-temporal
Postcentral_L	Calcarine_L	Hippocampus_L
2. Right frontal	Cuneus_L	ParaHippocampal_L
Precentral_R	Occipital_Sup_L	Amygdala_L
Frontal_Sup_R	Precuneus_L	Lingual_L
Frontal_Mid_R	Precuneus_R	Occipital_Inf_L
Frontal_Inf_Oper_R	Paracentral_Lobule_L	Occipital_Inf_R
Frontal_Inf_Tri_R	Paracentral_Lobule_R	Fusiform_L
Frontal_Sup_Medial_R	5. Occipital	Postcentral_R
3.Frontal-subcortical	Calcarine_R	Parietal_Sup_R
Frontal_Sup_Orb_L	Cuneus_R	Parietal_Inf_R
Frontal_Mid_Orb_L	Occipital_Sup_R	Angular_R
Frontal_Inf_Orb_L	Occipital_Mid_R	Heschl_R
Rolandic_Oper_L	6. Frontoorbital	Temporal_Sup_R
Olfactory_L	Frontal_Sup_Orb_R	Temporal_Pole_Sup_L
Olfactory_R	Frontal_Mid_Orb_R	Temporal_Mid_R
Frontal_Mid_Orb_L	Frontal_Inf_Orb_R	Temporal_Pole_Mid_L
Frontal_Mid_Orb_R	7. Right parieto-temporal	Temporal_Inf_L
Rectus_L	Rolandic_Oper_R	9. Temporal
Rectus_R	Insula_R	Temporal_Inf_R
Insula_L	Occipital_Mid_L	Hippocampus_R
Cingulum_Ant_L	Parietal_Sup_L	ParaHippocampal_R
Cingulum_Ant_R	Parietal_Inf_L	Amygdala_R
Caudate_L	SupraMarginal_L	Lingual_R
Putamen_L	SupraMarginal_R	Fusiform_R
Pallidum_L	Angular_L	Temporal_Pole_Sup_R
Thalamus_L	Caudate_R	Temporal_Pole_Mid_R
10. Cerebellum		
Vermis and Cerebellum regions in module		

hemisphere (7 regions of AAL atlas) while module *Central* chiefly includes the frontal lobe and premotor cortical regions comprising 13 regions of the AAL atlas (see Table 2 for detail).

Network Properties and Postoperative Outcome

In the depicted modules, the network parameters eccentricity, characteristic path length and global efficiency showed

an association with both the postoperative stimulation parameter (DBS voltage) for an optimal clinical response and the motor score ($UPDRS_{III}$). The computation of network metrics over the entire network did not predict the clinical outcome after DBS. In the modules with significant differences compared to the random network (*Left-frontal* and *Central*), eccentricity showed a significant interdependency with the DBS voltage (*Left-frontal*: $r = -0.36$, $p < 0.05$; *Central*: $r = -0.39$, $p < 0.05$). Eccentricity values from the *Left-frontal* and *Central* modules also correlated significantly with the postoperative motor outcome as defined from $UPDRS_{III}$ (module *Left-frontal*: $r = 0.47$; *Central*: $r = 0.45$, both $p < 0.05$) affirming the impact on the clinical state.

To determine the role of distinct anatomical regions within a module, we compared the AUC from the ROC analysis of eccentricity values from different areas within the module. In the module *Left-frontal*, we determined that the connectivity pattern from the medial superior frontal gyrus, primarily involved in executive functions, the dorsolateral superior frontal gyrus, and the opercular part of the inferior frontal gyrus could be used as classifiers to assess predictive model accuracy (Fig. 4).

In the module *Central*, the eccentricity in the frontal cortex and regions of the limbic network represented anatomical areas within the module with the best accuracy for effect delineation. In this module, the eccentricity values from the SMA, posterior cingulate gyrus, median cingulate and paracingulate gyrus were predictors for the optimal modeling accuracy (Fig. 5).

The correlation between the position of the electrode VTA mask and voltage or postoperative $UPDRS_{III}$ was not significant ($p > 0.1$). Furthermore, the permutation test (randomise tool in FSL) performed using the VTA masks and voltage and postoperative $UPDRS_{III}$ also did not yield any significant (i.e. $p < 0.05$, corrected) clusters.

Discussion

The proposed brain connectivity analysis and community detection methods revealed a significant association between the level of modular topology and connectivity in the frontal cortex and postoperative outcome after STN–DBS in PD patients. Patients with a more efficient (less degraded) network topology in the frontal cortex (with higher eccentricity in comparison with random network) would need less voltage to achieve the optimal motor response. MRI-derived connectivity measures might serve as important apparative and examiner independent predictors for the clinical DBS-outcome and might be used to optimize patient selection.

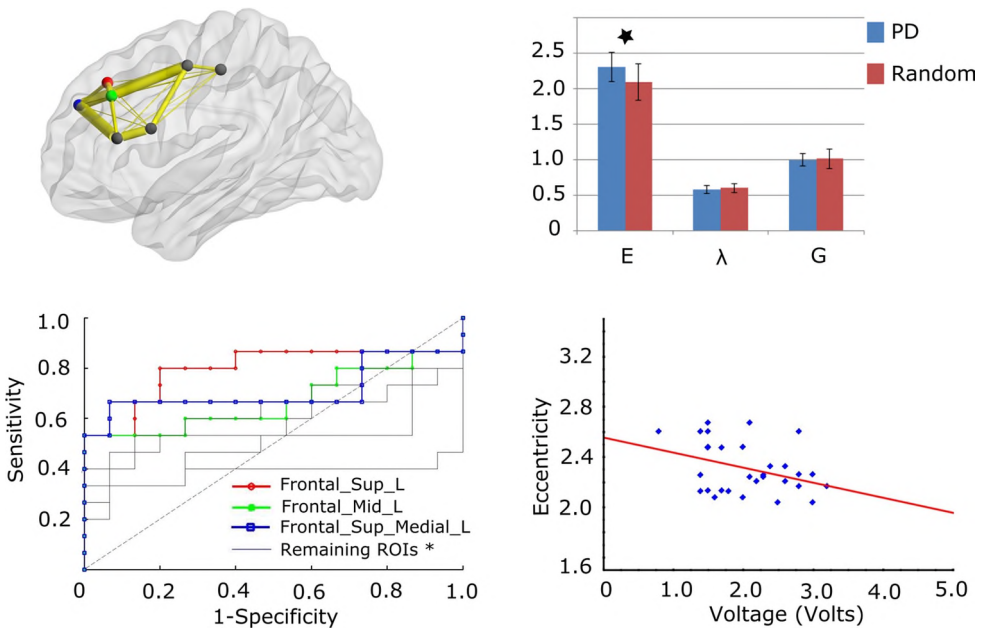

Fig. 4 Networks comparison in module 'Left frontal'. Figure in upper left shows the brain mesh and the included brain regions (spheres). Yellow lines indicate the weighted connectivity between them. Upper right: The histogram shows the difference in the network parameters mean with standard deviation from eccentricity (E), characteristic path length (λ) and global efficiency (G) of PD in comparison to random networks. The asterisk represents the statistically significant difference observed ($p < 0.05$). Lower left: ROC curves obtained from the regions within the module. The *sensitivity–specificity* plot was obtained from the analysis between the network measures from PD and random network. The highlighted lines show the regions in this module with the highest AUC. The plot on the lower right shows the correlation between eccentricity and DBS voltage in this module

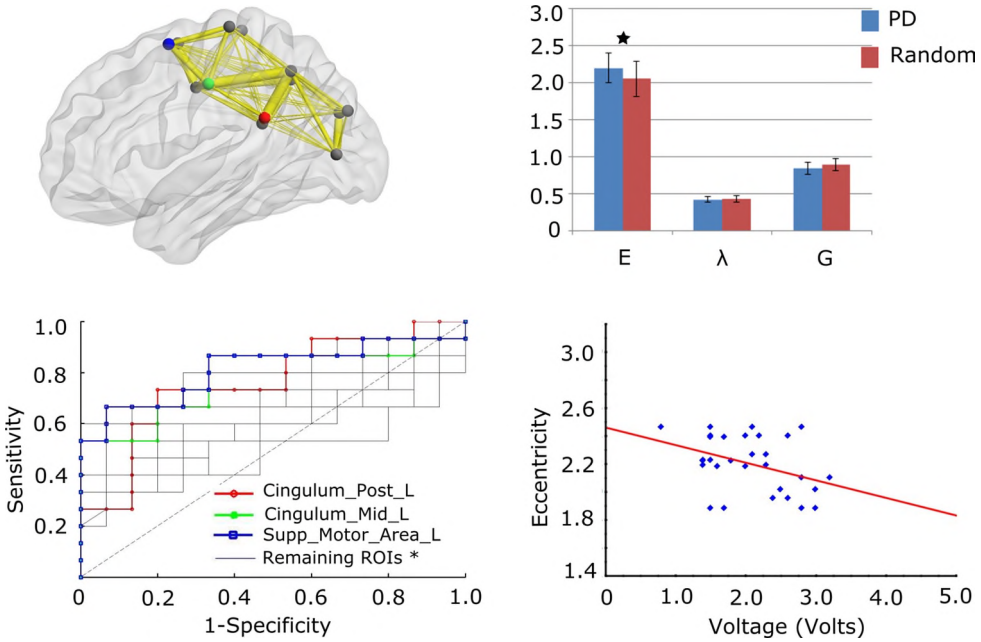

Fig. 5 Networks comparison in module 'Central'. Figure in upper left shows the brain mesh an the included brain regions (spheres). Yellow lines indicate the weighted connectivity between them. Upper right: The histogram shows the difference in the network parameters mean with standard deviation from eccentricity (E), characteristic path length (λ) and global efficiency (G) of PD in comparison to random networks. The asterisk represents the statistically significant difference observed ($p < 0.05$). Lower left: ROC curves obtained from the regions within the module. The *sensitivity–specificity* plot was obtained from the analysis between the network measures from PD and random network. The highlighted lines show the regions in this module with the highest AUC. The plot on the lower right shows the correlation between eccentricity and DBS voltage in this module

Network Structure Detection in Patients for STN–DBS

Brain functionality can be characterized by local interactions and a global integration in modules for specific brain functions (Park and Friston 2013). The modular and hierarchical organization to support the effectivity of brain functions has already been established non-invasively in humans as derived from structural and functional MRI network analyses (Sporns and Zwi 2004; van den Heuvel and Sporns 2011). It is obvious from the complex layered, modular and hierarchical cerebral organization that high frequency stimulation does not only affect the STN itself, but also distant areas. Furthermore, the complex interaction with the PD pathology is not only focused on substantia nigra or STN regions but encompasses an altered connectivity between interconnected regions comprising prefrontal, frontal and limbic regions. To improve actual and future therapeutic strategies an exact understanding of the complex interplay of PD pathology and local and global effects of actual therapy strategies i.e. STN–DBS is needed (Canu et al. 2015). Hence, the proposed community and modular structures analysis has the highly promising possibility of the exact characterisation of the interconnected networks that are reached by STN–DBS.

The revealed modules encompass prefrontal, frontal (SMA) and limbic cortex (cingulate and paracingulate cortex). The described network of prefrontal and frontal regions is mainly involved in executive functions and is impaired early in the disease course in PD patients (Nagano-Saito et al. 2005; Amboni et al. 2008; Koshimori et al. 2015). Direct connections of STN to these regions have been described (Brunenberg et al. 2012b). Two recent studies have shown the importance of these connections for STN–DBS efficiency, in Parkinsonian rats (Li et al. 2012) showed that STN–DBS activates the layer V neurons in the motor cortex, which contributes to the disruption of abnormal neural activities, while (Gradinaru et al. 2009) demonstrated a direct and therapeutically beneficial activation of motor and premotor areas with STN stimulation using optogenetics and solid-state optics. In humans, only indirect intimations regarding the distributed effects of DBS exist. Grey matter cortical thickness analysis on patients with PD has shown widespread cortical thinning in frontal and premotor regions in comparison to healthy controls (Pereira et al. 2012). In our previous study (Muthuraman et al. 2017), we found that the cortical integrity is affected mainly in frontal lobe (paracentral area and superior frontal region) and is correlated with DBS parameters and clinical outcome. Furthermore, a recent study has shown that the modulation of white matter tracts directed to the superior frontal gyrus and the thalamus is associated

with favorable clinical outcomes and may contribute to the therapeutic effects of STN–DBS (Vanegas-Arroyave et al. 2016). Our data demonstrates the role of the connectivity pattern in the frontal and central regions for the STN–DBS clinical response in patients with PD and presents a first and direct translational proof of the description of the targeted networks from animal models.

Anatomical Regions of Relevance for STN–DBS

Eccentricity is computed as the maximal shortest distance between two nodes (in this case two brain regions of interest). It is a measure which shows how reachable a brain region is from others in a specific module (Pavlopoulos et al. 2011). A module with higher eccentricity values has an architecture that permits a more efficient information transfer to other regions; in this way, regions exert a stronger influence over other ones and interact more efficiently. In this study, we demonstrate that eccentricity values in modules encompassing prefrontal, frontal and limbic cortex are negatively correlated with the DBS-electrode voltage. The location of the electrode contact in STN has been shown in previous studies to be directly associated with the improvements in the cardinal symptoms (tremor, rigidity etc.); with the best clinical outcome achieved by stimulation in the dorsolateral motor part of the STN (Voges et al. 2002; Herzog et al. 2004). In our previous study, we also showed that the precise targeting of the lateral region of the STN is essential for achieving sufficient stimulation efficacy (Wodarg et al. 2012). Although it is possible to identify the STN using MRI in image-guided surgery, it is still not feasible with the post-operative low resolution MRI or T1—MPRAGE or DWI sequences used in this study. The placement of the lead and choice of active electrode in the STN holds significant importance for the postoperative outcome. These could be tested with available probabilistic STN atlases however this would also be an approximation to the entire STN region and not only the focused sensori-motor part. Therefore we opted to calculate the COG of the registered VTA in order to confirm only minimal differences in the location of the active electrodes. In our study, the location of the active contacts for DBS stimulation for the patient group was not linked to the collective $UPDRS_{III}$ values or the applied voltage for the optimal postoperative outcome. This could be due to the minimal variation of the location of the active contacts between the subjects. Even though the computation of the VTA is the gold standard for the computation of the targeted neural tissue in DBS studies (McIntyre et al. 2004; Butson et al. 2007), with image processing and registration errors, further interpolations of absolute distances occur which is one limitation of the method and hence this study.

Predictive Effects of Network Degeneration and Comparison to Random Architecture

The human brain exhibits small-world topology, a favorable property for efficient information transfer (Stam 2004; Achard and Bullmore 2007). In addition, this topology is associated with improved cognitive and motor performance (Micheloyannis et al. 2006; van den Heuvel et al. 2009). Neurodegenerative disorders cause disturbances in the optimal organization of brain function and increase randomness in the network (van Straaten and Stam 2013). Functional networks in Alzheimer's disease lose their normal small-world structure and regress towards a more random architecture (Stam et al. 2007). The loss of overall functional connectivity and small-world properties with increased randomness of the network was also shown for individuals with schizophrenia (Liu et al. 2008; Yu et al. 2011). A reduced network efficiency has been shown in the functional network in PD patients by the aid of functional MRI (Skidmore et al. 2011). In our study, we observed that in modules encompassing frontal and central cortical areas, the eccentricity values in patients with PD were higher than that of the random network indicating the existence of small-world and hierarchical topology in those modules. The network reorganization with neurodegeneration toward architecture with less small-world properties and increased randomness motivated us to depict modules with highly organized topology in comparison to random networks. Hence, we observed that the effectiveness of STN–DBS is only depicted in modules where the network topology is preserved and hierarchical characteristics exist.

Conclusion

The performed network analysis revealed that connectivity properties of a network in the frontal and central regions are closely linked to the postoperative clinical outcome following STN–DBS. Eccentricity as a topological-characteristic of the network defining how cerebral regions are embedded in relation to distant sites shows a clear association between structural architecture and clinical outcome to functional DBS neuromodulation in PD. The implementation of connectivity profile analysis into the clinical setting might be an important tool to help define and improve the postoperative outcome.

Acknowledgements This work was supported by the German Research Foundation (DFG; CRC-TR-128).

References

Achard S, Bullmore E (2007) Efficiency and cost of economical brain functional networks. PLoS Comput Biol 3(2):e17

Amboni M, Cozzolino A, Longo K, Picillo M, Barone P (2008) Freezing of gait and executive functions in patients with Parkinson's disease. Mov Disord 23(3):395–400

Behrens TE, Berg HJ, Jbabdi S, Rushworth MF, Woolrich MW (2007) Probabilistic diffusion tractography with multiple fibre orientations: what can we gain? Neuroimage 34(1):144–155

Blondel VD, Guillaume JL, Lambiotte R, Lefebvre E (2008) Fast unfolding of communities in large networks. J Stat Mech 2008(10):10008

Brittain JS, Brown P (2014) Oscillations and the basal ganglia: motor control and beyond. Neuroimage 85:637–647

Brunenberg EJ, Moeskops P, Backes WH, Pollo C, Cammoun L, Vilanova A et al (2012a) Structural and resting state functional connectivity of the subthalamic nucleus: identification of motor STN parts and the hyperdirect pathway. PloS ONE 7(6):e39061

Brunenberg EJL, Moeskops P, Backes WH, Pollo C, Cammoun L, Vilanova A et al (2012b) Structural and resting state functional connectivity of the subthalamic nucleus: identification of motor STN parts and the hyperdirect pathway. PloS ONE 7(6):e39061

Bullmore E, Sporns O (2009) Complex brain networks: graph theoretical analysis of structural and functional systems. Nat Rev Neurosci 10(3):186–198

Butson CR, Cooper SE, Henderson JM, McIntyre CC (2007) Patient-specific analysis of the volume of tissue activated during deep brain stimulation. Neuroimage 34(17113789):661–670

Canu E, Agosta F, Sarasso E, Volonte MA, Basaia S, Stojkovic T et al (2015) Brain structural and functional connectivity in Parkinson's disease with freezing of gait. Hum Brain Mapp 36(12):5064–5078

Fukaya C, Yamamoto T (2015) Deep brain stimulation for parkinson's disease: recent trends and future direction. Neurologia Medico-Chirurgica 55(5):422–431

Girvan M, Newman MEJ (2002) Community structure in social and biological networks. Proc Natl Acad Sci USA 99(12):7821–7826

Gradinaru V, Mogri M, Thompson KR, Henderson JM, Deisseroth K (2009) Optical deconstruction of parkinsonian neural circuitry. Science 324(5925):354–359

Groppa S, Herzog J, Falk D, Riedel C, Deuschl G, Volkmann J (2014) Physiological and anatomical decomposition of subthalamic neurostimulation effects in essential tremor. Brain 137(Pt 1):109–121

Haynes WI, Haber SN (2013) The organization of prefrontal-subthalamic inputs in primates provides an anatomical substrate for both functional specificity and integration: implications for *Basal Ganglia* models and deep brain stimulation. J Neurosci 33(11):4804–4814

Herzog J, Fietzek U, Hamel W, Morsnowski A, Steigerwald F, Schrader B et al (2004) Most effective stimulation site in subthalamic deep brain stimulation for Parkinson's disease. Mov Disord 19(9):1050–1054

Jenkinson M, Smith S (2001) A global optimisation method for robust affine registration of brain images. Med Image Anal 5(2):143–156

Jenkinson M, Bannister P, Brady M, Smith S (2002) Improved optimization for the robust and accurate linear registration and motion correction of brain images. Neuroimage 17(2):825–841

Johansen-Berg H, Behrens TE, Robson MD, Drobnjak I, Rushworth MF, Brady JM et al (2004) Changes in connectivity profiles define functionally distinct regions in human medial frontal cortex. Proc Natl Acad Sci USA 101(36):13335–13340

Klingelhoefer L, Samuel M, Chaudhuri KR, Ashkan K (2014) An update of the impact of deep brain stimulation on non motor symptoms in Parkinson's disease. J Parkinson's Dis 4(2):289–300

Koshimori Y, Segura B, Christopher L, Lobaugh N, Duff-Canning S, Mizrahi R et al (2015) Imaging changes associated with cognitive abnormalities in Parkinson's disease. Brain Struct Funct 220(4):2249–2261

Latora V, Marchiori M (2001) Efficient behavior of small-world networks. Phys Rev Lett 87(19):198701

Li Q, Ke Y, Chan DCW, Qian ZM, Yung KKL, Ko H et al (2012) Therapeutic deep brain stimulation in Parkinsonian rats directly influences motor cortex. Neuron 76(5):1030–1041

Liu Y, Liang M, Zhou Y, He Y, Hao Y, Song M (2008) et al. Disrupted small-world networks in schizophrenia. Brain 131(Pt 4):945–961

McIntyre CC, Hahn PJ (2010) Network perspectives on the mechanisms of deep brain stimulation. Neurobiol Dis 38(3):329–337

McIntyre CC, Mori S, Sherman DL, Thakor NV, Vitek JL (2004) Electric field and stimulating influence generated by deep brain stimulation of the subthalamic nucleus. Clinical Neurophysiol 115(3):589–595

Meunier D, Achard S, Morcom A, Bullmore E (2009) Age-related changes in modular organization of human brain functional networks. Neuroimage 44(3):715–723

Micheloyannis S, Pachou E, Stam CJ, Vourkas M, Erimaki S, Tsirka V (2006) Using graph theoretical analysis of multi channel EEG to evaluate the neural efficiency hypothesis. Neurosci Lett 402(3):273–277

Muthuraman M, Deuschl G, Koirala N, Riedel C, Volkmann J, Groppa S (2017) Effects of DBS in parkinsonian patients depend on the structural integrity of frontal cortex. Scientific Rep 7:43571

Nagano-Saito A, Washimi Y, Arahata Y, Kachi T, Lerch J, Evans A et al (2005) Cerebral atrophy and its relation to cognitive impairment in Parkinson disease. Neurology 64(2):224–229

Nambu A, Chiken S (2015) Mechanism of DBS: inhibition, Excitation, or Disruption? In: Itakura T (ed) Deep brain stimulation for neurological disorders: theoretical background and clinical application. Springer International Publishing, Cham, pp 13–20

Newman MEJ (2006) Modularity and community structure in networks. Proc Natl Acad Sci USA 103(23):8577–8582

Odekerken VJJ, van Laar T, Staal MJ, Mosch A, Hoffmann CFE, Nijssen PCG et al (2013) Subthalamic nucleus versus globus pallidus bilateral deep brain stimulation for advanced Parkinson's disease (NSTAPS study): a randomised controlled trial. Lancet Neurol 12(1):37–44

Olde Dubbelink KT, Hillebrand A, Stoffers D, Deijen JB, Twisk JW, Stam CJ et al (2014) Disrupted brain network topology in Parkinson's disease: a longitudinal magnetoencephalography study. Brain 137(Pt 1):197–207

Opsahl T, Colizza V, Panzarasa P, Ramasco JJ (2008) Prominence and control: the weighted rich-club effect. Phys Rev Lett 101:168702

Park H-J, Friston K (2013) Structural and functional brain networks: from connections to cognition. Science 342(6158):1238411

Pavlopoulos GA, Secrier M, Moschopoulos CN, Soldatos TG, Kossida S, Aerts J et al (2011) Using graph theory to analyze biological networks. BioData Mining 4:10

Pereira JB, Ibarretxe-Bilbao N, Marti M-J, Compta Y, Junqué C, Bargallo N et al (2012) Assessment of cortical degeneration in patients with Parkinson's disease by voxel-based morphometry, cortical folding, and cortical thickness. Hum Brain Mapp 33(11):2521–2534

Pereira JB, Aarsland D, Ginestet CE, Lebedev AV, Wahlund LO, Simmons A et al. (2015) Aberrant cerebral network topology and mild cognitive impairment in early Parkinson's disease. Hum Brain Mapp 36(8):2980–2995

Ranck JB (1975) Which elements are excited in electrical stimulation of mammalian central nervous system: a review. Brain Res 98(3):417–440

Ritchey M, Yonelinas AP, Ranganath C (2014) Functional connectivity relationships predict similarities in task activation and pattern

information during associative memory encoding. J Cogn Neurosci 26(5):1085–1099

Rubinov M, Sporns O (2010) Complex network measures of brain connectivity: uses and interpretations. Neuroimage 52(3):1059–1069

Skidmore F, Korenkevych D, Liu Y, He G, Bullmore E, Pardalos PM (2011) Connectivity brain networks based on wavelet correlation analysis in Parkinson fMRI data. Neurosci Lett 499(1):47–51

Sporns O (2003) Graph theory methods for the analysis of neural connectivity patterns. In neuroscience databases. Springer, New York, pp. 171–185

Sporns O, Zwi JD (2004) The small world of the cerebral cortex. Neuroinformatics 2(2):145–162

Stam CJ (2004) Functional connectivity patterns of human magnetoencephalographic recordings: a 'small-world' network? Neurosci Lett 355(1–2):25–28

Stam CJ, Jones BF, Nolte G, Breakspear M, Scheltens P (2007) Small-world networks and functional connectivity in Alzheimer's disease. Cereb Cortex 17(1):92–99

Stam CJ, de Haan W, Daffertshofer A, Jones BF, Manshanden I, van Cappellen van Walsum AM et al (2009) Graph theoretical analysis of magnetoencephalographic functional connectivity in Alzheimer's disease. Brain 132(1):213–224

Stein E, Bar-Gad I (2013) Beta oscillations in the cortico-basal ganglia loop during parkinsonism. Exp Neurol 245:52–59

Tzourio-Mazoyer N, Landeau B, Papathanassiou D, Crivello F, Etard O, Delcroix N et al (2002) Automated anatomical labeling of activations in SPM using a macroscopic anatomical parcellation of the MNI MRI single-subject brain. Neuroimage 15(1):273–289

Udupa K, Chen R (2015) The mechanisms of action of deep brain stimulation and ideas for the future development. Prog Neurobiol 133:27–49

van Straaten ECW, Stam CJ (2013) Structure out of chaos: functional brain network analysis with EEG, MEG, and functional MRI. Eur Neuropsychopharmacol 23(1):7–18

van den Heuvel MP, Sporns O (2011) Rich-Club organization of the human connectome. J Neurosci 31(44):15775–15786

van den Heuvel MP, Stam CJ, Kahn RS, Pol HE (2009) Efficiency of functional brain networks and intellectual performance. J Neurosci 29(23):7619–7624

Vanegas-Arroyave N, Lauro PM, Huang L, Hallett M, Horovitz SG, Zaghloul KA et al. (2016) Tractography patterns of subthalamic nucleus deep brain stimulation. Brain 139(4), 1200–1210.

Voges J, Volkmann J, Allert N, Lehrke R, Koulousakis A, Freund HJ et al. (2002) Bilateral high-frequency stimulation in the subthalamic nucleus for the treatment of Parkinson disease: correlation of therapeutic effect with anatomical electrode position. J Neurosurg 96(2):269–279

Weaver FM, Follett KA, Stern M, Luo P, Harris CL, Hur K et al (2012) Randomized trial of deep brain stimulation for Parkinson disease Thirty-six-month outcomes. Neurology 79(1):55–65

Witt K, Granert O, Daniels C, Volkmann J, Falk D, van Eimeren T et al (2013) Relation of lead trajectory and electrode position to neuropsychological outcomes of subthalamic neurostimulation in Parkinson's disease: results from a randomized trial. Brain 136(7):2109–2119

Wodarg F, Herzog J, Reese R, Falk D, Pinsker MO, Steigerwald F et al (2012) Stimulation site within the MRI-defined STN predicts postoperative motor outcome. Mov Disord 27(7):874–879

Yu Q, Sui J, Rachakonda S, He H, Gruner W, Pearlson G et al (2011) Altered topological properties of functional network connectivity in schizophrenia during resting state: a small-world brain network study. PloS ONE 6(9):e25423